EULER FLOW ANALYSIS OF SUPERSONIC TRANSPORT AIRCRAFT CONFIGURATIONS FOR AERODYNAMIC OPTIMIZATION IN TRANSONIC AND SUPERSONIC REGIMES

Carlo de Nicola, Renato Tognaccini
Dipartimento di Progettazione Aeronautica
Universita` degli Studi di Napoli, Italia

Alessandro Amendola, Luigi Paparone
CIRA - Centro Italiano di Ricerche Aerospaziali
Capua (CE), Italia

Pier Luigi Vitagliano
Alenia Aeronautica/DTT
Pomigliano d'Arco (NA), Italia

Abstract

The aim of the present paper is to show the results of an evaluation study concerning the ability of a general Euler/TLNS flow simulation system to deal with the inviscid analysis of complex SCT type configurations in transonic and supersonic conditions. Furthermore the capability of the Euler model to predict non linear effects in supersonic flow around wings with sharp and blunt leading edges is investigated and discussed.

List of symbols

r_c:	curvature radius of airfoil leading edge
c:	wing cord length
M_∞:	free-stream Mach number
α:	angle of attack
c_L:	lift coefficient
c_D:	drag coefficient
$c_{L\alpha}$:	lift curve slope
Δc_D:	drag due-to-lift coefficient
AR:	aspect ratio
S_s:	suction parameter
c_p:	pressure coefficient
c_N:	normal force coefficient
c_A:	axial force coefficient

Introduction

A re-newed interest in a second generation supersonic commercial transport (SCT-II) has stimulated Industries, Research Institutions and Universities to re-analyse new and old problems related to Supersonic Aerodynamics. This discipline will play a key role in the ambitious task to satisfy the very stringent requirements imposed to the overall performance of SCT in order to be economically viable. For instance, aerodynamic efficiency at all the flight envelope is one of the parameters that must be maximised to bound design constraints such as MTOW, range and environmental impact.

Today aerodynamicists can rely upon new tools, such as CFD, to improve design standards and achieve better results in terms of aerodynamic characteristics. In this paper we show results concerning the extension of a general complete multiblock structured zonal Euler/Thin-Layer Navier-Stokes simulation system to deal with inviscid supersonic flows. This system was initially developed for the analysis of subsonic/transonic regimes and was addressed to handle very complex aerodynamic configuration and a variety of flow features like inlet-outlet, propeller effects, etc. As matter of fact this system represents a well known, complete technological platform characterised by efficiency, versatility and engineering accuracy for the range of problems was designed for. Therefore it was considered worthwhile the extension of present system to the simulation of high speed flows.

In a previous work[1], the ability of the existing simulation system to analyse complex supersonic configurations was verified. At first it was payed attention to the grid generation process, that is the capability to produce 3D grids around complex shapes in a reasonable turn-around time. This would allow the use of such CFD tools since preliminary design phase. It is worth to mention that in general grid topology and quality should always be carefully controlled to ensure the desired level of numerical accuracy. Moreover the limits of the central space discretization used in the flow solver were

investigated with respect to the obtainable accuracy in the simulation of flows dominated by oblique shocks. By modifying the inviscid wall boundary conditions according to characteristic theory the algorithm provided sufficiently accurate solutions in the range of Mach number of interest for the SCT aircraft ($M_\infty < 3.0$).

In the present work transonic and supersonic flow calculations have been performed successfully around an Alenia SCT baseline configuration and preliminary results are reported for a wing-body-tail and a wing-body-tail-nacelle configuration.

Furthermore, in the second part of the paper, wing analysis has been carried out in order to assess the flow solution accuracy with respect to evaluation of non linear effects at supersonic speed like leading edge thrust and vortex flow development. Carlson[2] showed that these effects are relevant both from the point of view of local flow features (pressure distribution) and global characteristics (lift, drag). Today semi-empirical corrections to linear methods are available[3] for the evaluations of such effects, but it is widely recognised that further improvements are necessary.

As stated by Carlson it is still not clear if the leading edge thrust phenomenon can be described by the Euler model. In (4) we presented Euler results around an arrow wing with sharp leading edge in which a certain level of thrust was clearly determined provided that grids satisfy particular smoothness requirements. In this paper further studies have been carried out for wings with blunt leading edges.

Flow Simulation

The flow simulation system consists of software modules, which perform the main tasks of the aerodynamic simulation process:

- domain decomposition,
- grid generation,
- flow simulation,
- flow data visualisation and analysis.

The system is based on multi-block structured grids, i.e. the flow domain is subdivided in volumes (blocks) which are topologically equivalent to the unit cube, where the grid generation can be more easily performed. This task is carried out by the domain modeller[5]. It is possible to handle multi-connected regions and to control the grid shape by using a large amount of blocks. The blocks are connected to each other by faces. It is allowed to compound two faces into a so-called compound face, in order to connect two or more blocks to one block. The topological connections are completely defined when a table is given, containing a list of 6 faces for each block, a list of 4 edges for each face and a list of 2 vertices for each edge. The compound entities (edges and faces) require an additional list of two sub-entities. Some rules have to be checked in order to ensure consistency of the topological construction, and to avoid undesired gaps. The sequence of 6 faces in the definition list of a block defines also the computational co-ordinate direction within the block.

The geometry of the flow domain is defined when each vertex is associated to a 3D point in the physical space, each edge to a space curve and each face to a 3D surface, bounded by the face edges. Default edges are straight line connecting the edge vertices; non default edges are a chain of cubic Hermite polynomials, connecting a set of control points. Default faces are bi-linear transfinite interpolations of the face edges, while non-default faces are a set of bi-cubic Hermite polynomials, connecting a lattice of control-points. Most of the edges and faces in the flow domain are default ones. Non-default entities are usually located on the configuration. The geometry of a block is defined as a tri-linear transfinite interpolation of the block faces.

Input data to the system are the 3D points co-ordinates located on the configuration surfaces. Those are not necessarily the same 3D points that define the topological entities, since re-shaping and re-facing capabilities are built in the domain modeller. When the domain decomposition is completed, two files are produced, containing the topological tables and the geometrical definitions of the entities, which are input data to the grid generator.

The grid generation work consists of two sub-tasks[6]: setting the basic edge dimensions and grid tuning. The basic edge dimension is the number of cells to be produced along each block edge to get a continuous grid across block faces. The computational grid is produced from the basic grid, multiplying the edge dimensions by a power of two. Local grid refinement is possible on a block base. Grid tuning is mainly performed by algebraic techniques. The grid density and stretching can be assigned at the edge vertices by various means. A bi-harmonic solver can be used in the block faces to get orthogonality of the grid lines at the face edges. Different generation techniques are available within faces and blocks, which gives more flexibility. When the grid generation is completed, a file is produced, containing the grid point co-ordinates in each block and the topological connection tables , which are necessary to set the boundary conditions for the flow computation.

The flow simulation is performed by a multi-zone solver[7], which, in the present case, is used to solve the steady Euler equations in the whole domain. The space discretization is based on finite volumes, central schemes, with self-adaptive explicit 2nd and 4th order artificial dissipation terms[8]. Convergence toward the steady solution is achieved by an explicit Runge-Kutta pseudo-time stepping, with multi-grid acceleration technique. Residual averaging and enthalpy damping can be used to improve the convergence rates. The flow solver was proved to be effective in subsonic and transonic regimes.

For supersonic flow the application of centred schemes is more critical. Large oscillations caused by the explicit artificial dissipation can appear near shocks and can

considerably deteriorate the accuracy of the computed solutions especially when the flow is shock dominated. A significant improvement in the accuracy was achieved in case of interaction of oblique shocks with a slip wall by using numerical boundary conditions for wall simulation based on the characteristic theory[1]. Therefore the efficiency of central space discretization makes this approach competitive with modern shock capturing schemes especially for aerodynamic analysis of complex fields discretized with large grids.

Complex Configuration Analysis

The capability of the current flow simulation system to analyse complex geometries has been verified on a SCT type configuration designed by Alenia/DTT. Two grids are presented. The first one has been built around a wing-body-tail configuration, while in the second case four wing mounted nacelles have been added.

The definition of the domain decomposition was guided by the requirement to enable a simple upgrade of the topology. An H-structure has been chosen in the symmetry an in the wing planes, while the O-topology is used in the front planes.

The clean wing topology is built up by 42 blocks for the half configuration and is illustrated in fig. 1. The nacelle installation considerably increases the complexity of the topology and the domain decomposition required the definition of 94 blocks.

The number of grid cells on the finer grid level for the nacelle mounted configuration is 444,416 with the wing airfoil described by 129 grid points.

Some details of the final grids are presented in fig. 2-4.

A typical example of convergence history of the flow solution is shown in fig. 5, in which the root mean square and the maximum residual of mass equation are plotted versus time iterations.

The supersonic flow analysis has been mainly performed at the design cruise condition $M_\infty = 2.0$. The isobars in the symmetry plane and on the configuration are shown for the nacelle mounted case in fig. 6, while the wing isobars and pressure coefficient distribution for the clean wing case are presented in fig. 7.

A first qualitative analysis of the results gives a reasonable level of confidence with the computed solutions, based upon numerical parameters such as average residual, numerical artificial dissipation and physical parameters such as pressure distributions, lift and drag coefficients, the last one compared with linear prediction methods[9].

One of the main features of the present flow simulation system is the capability to analyse an SCT type configuration in a large part of the flight envelope (sub-trans-supersonic). In particular in fig. 8 it is plotted the computed drag (wave + lift) versus free-stream Mach number at fixed incidence ($\alpha = 3^o$).

In spite of the lack of experimental data to validate present results, these tests were very useful to assess the possibility to perform extensive analysis of quite complex aerodynamic shapes even during the early stages of the aerodynamic design process with acceptable turn-around time and engineering accuracy.

Non linear effects in supersonic flows

The purpose of the present section is to verify the possibility of Euler simulations to contribute to the assessment of aerodynamic non linear effects at supersonic cruise conditions, in particular vortex development and supersonic leading edge thrust. Both effects are of primary importance even if the first one (vortex) could be small. As far as the leading edge thrust is concerned, it is generally recognised that a correct evaluation of leading edge suction would be very useful during the aerodynamic optimisation of the aircraft configuration.

In the present work two supersonic wings with the same planform have been investigated and the results have been compared with the available experimental data[10]. They are characterised by different airfoil sections with sharp and blunt leading edge respectively. The computed force coefficients are compared with experiments and with the results of Carlson method that is based on the linearized theory integral equations with semi-empirical correction for taking into account non linear effects.

The main wing characteristics are the following:

- AR = 3.55;
- variable leading edge sweep angle (60 to 54 degrees);
- taper ratio equal to 0.11;
- 4% airfoil thickness;
- sharp leading edge $r_e/c = 0.0$;
- blunt leading edge $r_e/c = 0.0047$.

The leading edge is unswept in order to achieve a constant value of 100% leading edge thrust from half-semispan to tip.

The grid topology used for both the sharp and blunt wings is C-type in the symmetry plane and O-type in the front plane. Only six blocks have been defined for a total number of 256,000 grid cells; the upper and lower wing surfaces have been both discretized with 1920 grid cells. In fig. 9 the symmetry plane and the wing surface grid are presented for the blunt wing.

The wings have been analysed for the following free stream conditions:

- subsonic leading edge case,
  $M_\infty = 1.6, \alpha = (0, 1, 2, 4, 5, 6, 8^\circ)$;

- supersonic leading edge case,
  $M_\infty = 2.16, \alpha = (0, 1, 2, 4, 5, 6, 8^\circ)$.

The wind tunnel model of the sharp configuration had a very small curvature radius at the leading edge (r_e/c = 0.0005); this value was also used for the thrust evaluation

by the linear method. The experiments were performed at Reynolds=$2x10^6$.

As expected the computed pressure distributions near the leading edge region show significative differences between the blunt and the sharp cases. The comparison between the upper wing isobars in case of subsonic and supersonic leading edge tests are shown in fig. 10, while pressure distributions at different span sections are presented for the $M_\infty = 1.6; \alpha = 5°$ case in fig. 11, both for the sharp and blunt wing. Particular care has to be taken in the analysis of the blunt leading edge flow. In fact, it is well known that in such a case, if a primary vortex separation is computed, it is only related to the artificial dissipation and to the grid used in the flow computations, since separation is not fixed at leading edge as in the sharp case[11]. Therefore an agreement with experiments can be expected only at low incidence for the blunt case.

In this context it is interesting to look more in detail the evaluation of force coefficients. They have been computed by integration of surface pressure distribution; friction drag effects, based on flat plate assumption, have been added in order to compare data with experiments.

To quantify the amount of leading edge thrust it is useful to introduce the suction parameter[2]:

$$S_s = \frac{C_L \cdot \tan(C_L/C_{L\alpha}) - \Delta C_D}{C_L \cdot \tan(C_L/C_{L\alpha}) - C_L^2/(\pi \cdot AR)}$$

With such parameter the computed drag is compared with the upper bound (drag of a flat wing with no thrust and vortex forces) and a lower bound obtained in case of a wing with an elliptical span load distribution and the full amount of theoretical leading edge thrust. These two limit cases are obtained respectively for S_s=0 and S_s=1.

Subsonic leading edge

The results are plotted in fig. 12 for both wings; the agreement with the experiments is quite satisfactory in the range of moderate incidence studied in this work. The behaviour of the axial force coefficient computed by the Euler solver, that is diminishing with the angle of attack, shows that a certain amount of leading edge thrust is predicted. This is different from what linear theory does; in fact linearized methods assume the invariance of the axial force with respect to incidence. Euler separated flow at leading edge is present for the sharp case while no separation has been detected near the blunt leading edge. For the last case the origin of the computed suction is essentially due to an accelerated flow over the nose without separation. This phenomenon is confined to cruise conditions and moderate lift.

The comparison with the experiments shows that the predicted wave drag at 0-lift is in good agreement. The Euler flow solver overestimates drag with respects to experiments. This problem is related to an underestimation of thrust as shown by the suction parameter behaviour. Improved accuracy is expected by reducing the artificial numerical dissipation introduced in the flow calculations.

Supersonic leading edge

Similar results have been obtained in case of supersonic leading edge flow as shown in fig. 13.

The modified linear theory assumes in this case zero thrust. The Euler calculations and the experiments agree in the prediction of a positive thrust for the sharp wing, while provide negative effects for very low incidence for the blunt case.

The possibility to quantify non linear effects by the Euler model, at least for comparing different wing configurations, allows to overcome some of the limit of linear theory. In particular the semi-empirical correction provides satisfactory results when the wing shape is similar to the one used in the experimental data correlation, i.e. arrow wings with constant sweep[9].

Conclusions

The ability of a general Euler/TLNS flow simulation to deal with supersonic speeds has been demonstrated. The system allows the user to decompose the domain and generate the 3D grid around a complete SCT aircraft configuration within a reasonable amount of time and with a minimum expertise. Successively the flow solution can be computed at cruise conditions both at subsonic, transonic or supersonic speeds with only a minor effort required to adapt the grid. Furthermore the capability of the Euler flow model to predict non linear effects in supersonic flows has been investigated. These effects play a key role in the optimisation of drag-due-to-lift of next generation supersonic transport.

The main results of the present analysis can be summarised as follows:

- the Euler model is able to detect leading edge thrust for both wings with sharp and blunt leading edges, with an improved level of accuracy with respect to corrected linear methods;

- Euler leading edge thrust is underestimated with respect to experiments and in addition it is particularly sensitive to grid quality;

- at low angles of attack the Euler model also improves the quality of solution in terms of pressure distribution with respect to linear methods;

- in general first order effects in the force coefficients evaluation are well predicted;

- further investigations are required in the fields of solution grid dependency, inclusion of viscous effects,

extension to the analysis of different flow type regimes according to the Stanbrook and Squire classification[12].

References

1. A. Amendola, C. de Nicola, R. Tognaccini, P.L. Vitagliano, Aerodynamic Analysis around Complex Aircraft Configurations by an Euler Multiblock Structured Flow Simulation System in Subsonic, Transonic and Supersonic Flow Regimes, Proc. Conf. on Recent Development and Applications in Aeronautical CFD, Bristol (UK), 1993.
2. H.W. Carlson, M.J. Mann, Survey and Analysis of Research on Supersonic Drag-Due-to-Lift Minimization with Recommendations for Wing Design, NASA TP-3202, 1992.
3. H.W. Carlson, R.J. Mack, Estimation of Leading Edge Thrust for Supersonic Wings of Arbitrary Planform, NASA TP-1270, 1978.
4. C. de Nicola, R. Tognaccini, P. Visingardi, L. Paparone, Progress in the Aerodynamic Analysis of Inviscid Supersonic Flow Fields around Complex Aircraft Configurations, AIAA 94-1821, 12th AIAA Applied Aerodynamics Conference, Colorado Springs (USA), 1994.
5. J.W. Boerstoel, S.P. Speckreijse, P.L. Vitagliano, The Design of a System of Codes for Industrial Calculations of Flows around Aircraft and Other Complex Aerodynamic Configurations, AIAA 92-2619, 10th Applied Aerodynamics Conf., Palo Alto (USA), 1992.
6. S.P. Speckreijse, J.W. Boerstoel, P.L. Vitagliano, New Concepts for Multi-Block Grid Generation for Flow Domains around Complex Aerodynamic Configurations, Proc. 3rd Inter. Conf. on Numerical Grid Generation in CFD and Related Fields, Barcelona, 1991.
7. J.W. Boerstoel, A. Kassies, J.C. Kok, M. Amato, R. Tognaccini, Predesign of ENSOLV; a Code for the Numerical Simulation of 3D Flows Using the Thin-Layer Navier-Stokes/Euler Equations, NLR CR-91243, 1991.
8. A. Jameson, W. Schmidt, E. Turkel, Numerical Solutions of the Euler Equations by Finite Volume Methods Using Runge-Kutta Time-Stepping Schemes, AIAA 81-1259, Palo Alto (USA), 1981.
9. M. Averardo, High-Speed Civil Transport Aerodynamic Study of SCT-3 Configuration, Alenia NT 58x93005, 1994.
10. R.J. Mack, Wind-Tunnel Investigation of Leading-edge Thrust on Arrow Wings in Supersonic Flow, NASA TP-2167, 1983.
11. R.W. Newsome, O.A. Kandil, Vortical Flow Aerodynamics-Physical Aspects and Numerical Simulation, AIAA 87-0205, AIAA 25th Aerospace Sciences Meeting, Reno (USA), 1987.
12. A. Stanbrook, L.C. Squire, Possible Types of Flow at Swept Leading Edges, Aeron. Q., vol. XV, pt. 1, 1964.

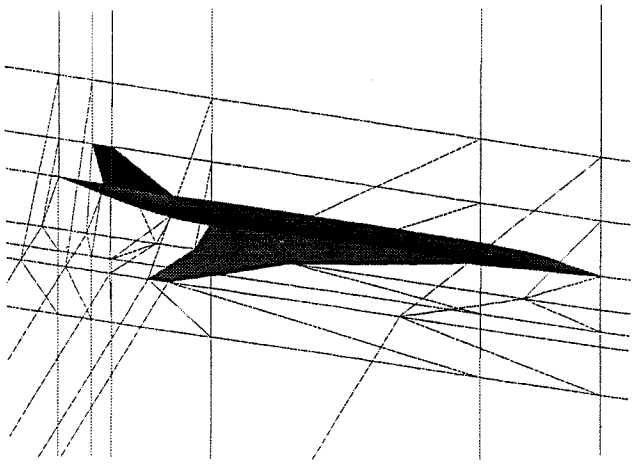

Fig. 1
Topology of the wing-body-tail SCT configuration

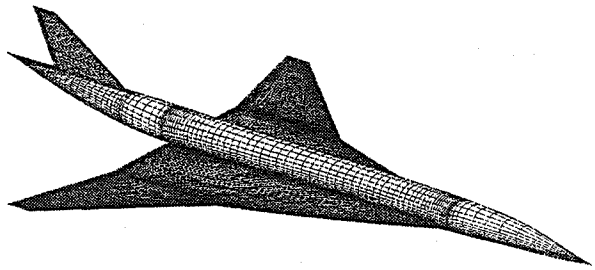

Fig. 2
Surface grid of the wing-body-tail SCT configuration

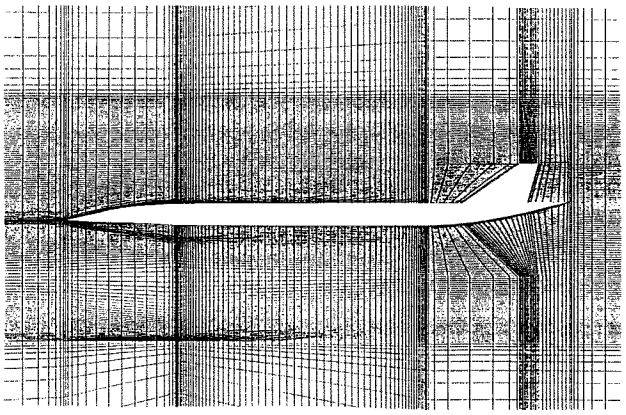

Fig. 3
Symmetry plane grid of the wing-body-tail SCT configuration

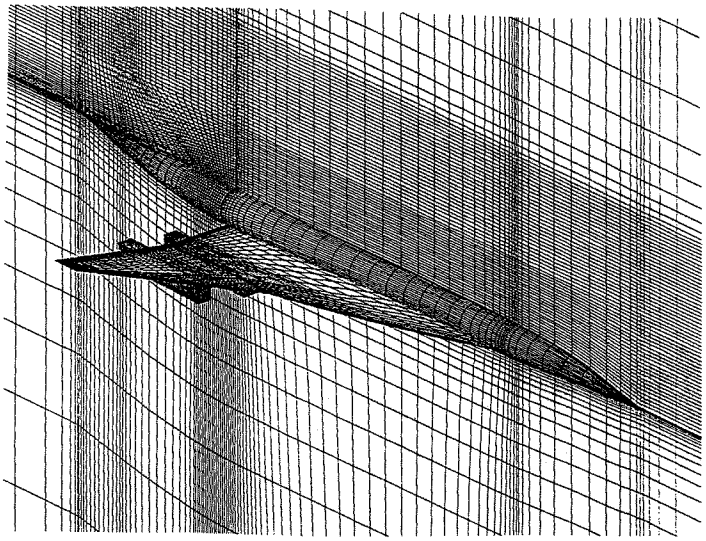

Fig. 4
3D view of the grid around
the wing-body-tail-nacelle SCT configuration

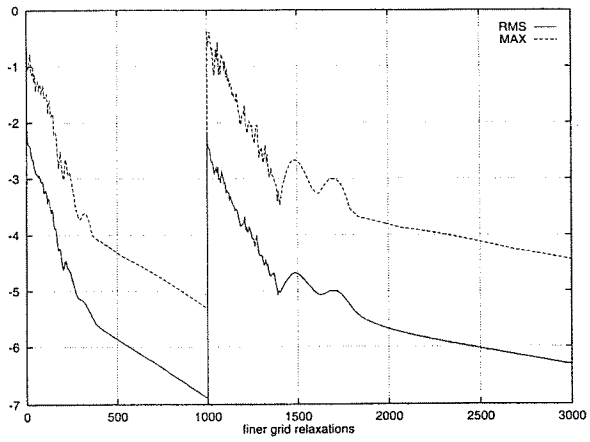

Fig. 5
Convergence history
wing-body-tail SCT configuration test
$M_\infty = 2.0, \alpha = 3^\circ$

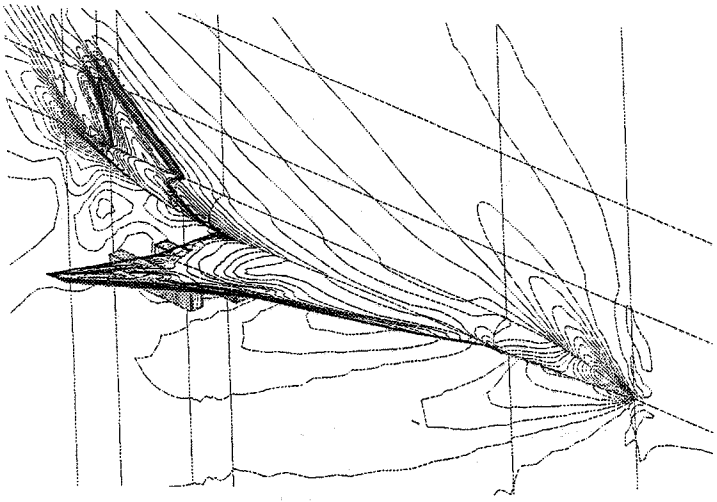

Fig. 6
3D view of the computed flow field (isobars)
around the wing-body-tail-nacelle SCT configuration
$M_\infty = 2.0, \alpha = 3^\circ$

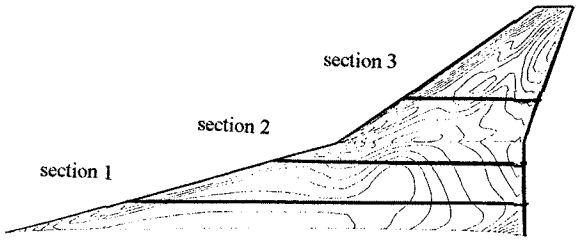

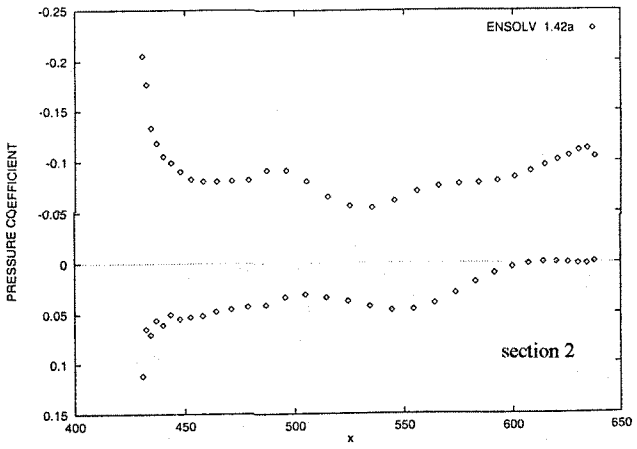

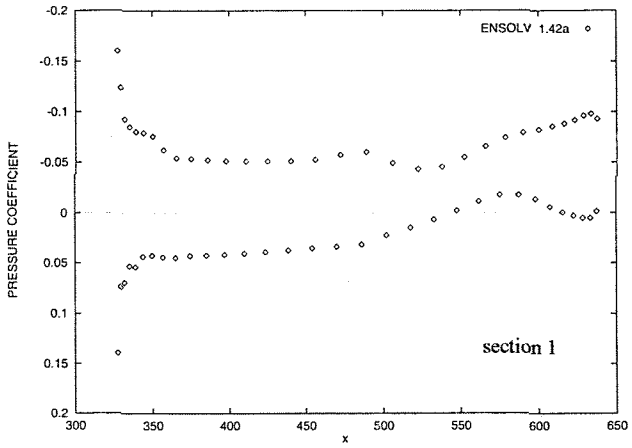

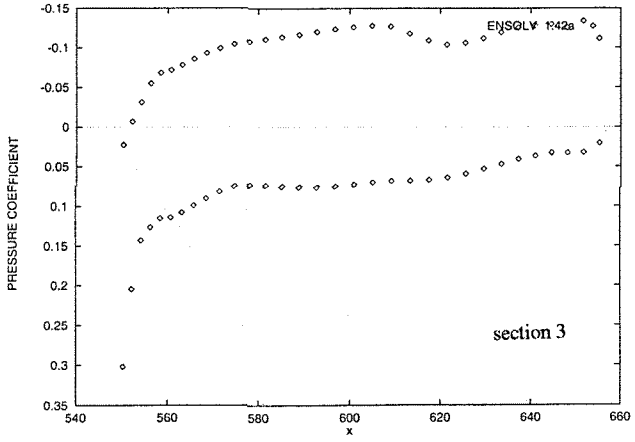

Fig. 7
Pressure coefficient distribution on the upper wing
of wing-body-tail SCT configuration
$M_\infty = 2.0, \alpha = 3^\circ$

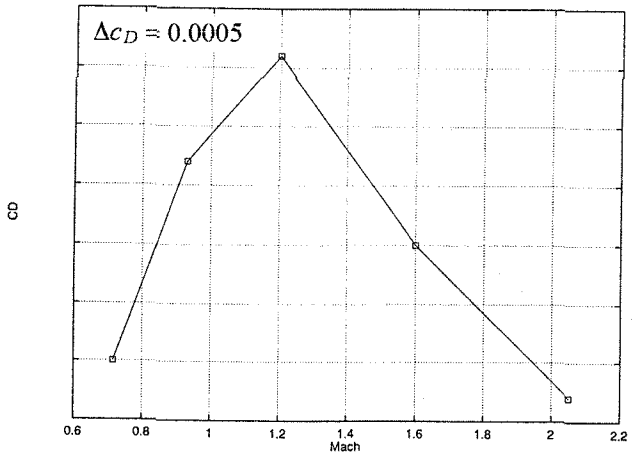

Fig. 8
Drag coefficient versus Mach number
wing-body-tail SCT configuration

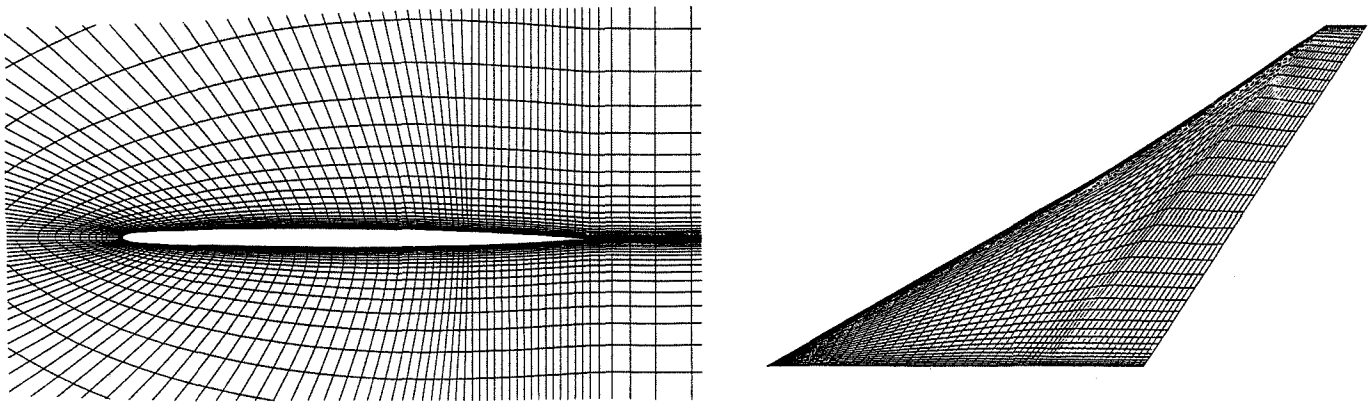

Fig. 9
Grid around the blunt leading edge wing

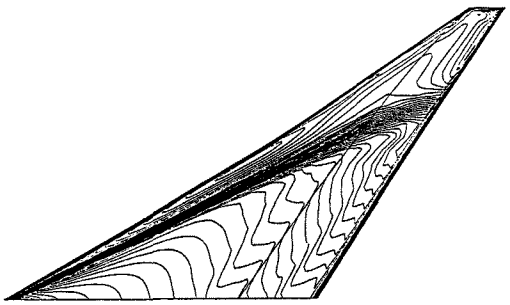

(a)
sharp leading edge wing
$M_\infty = 1.6, \alpha = 5°$

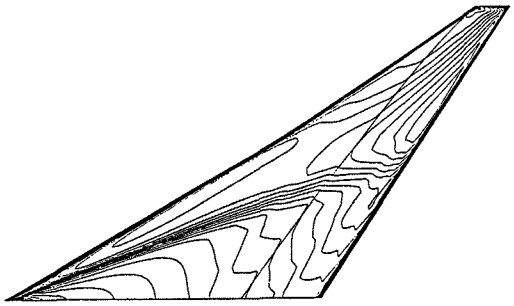

(c)
blunt leading edge wing
$M_\infty = 1.6, \alpha = 5°$

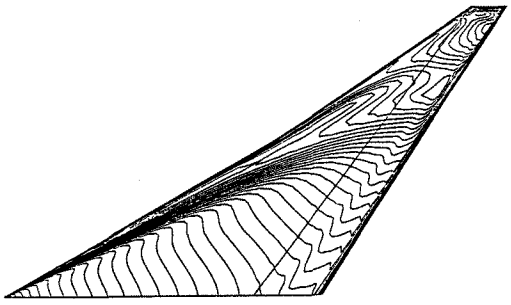

(b)
sharp leading edge wing
$M_\infty = 2.16, \alpha = 5°$

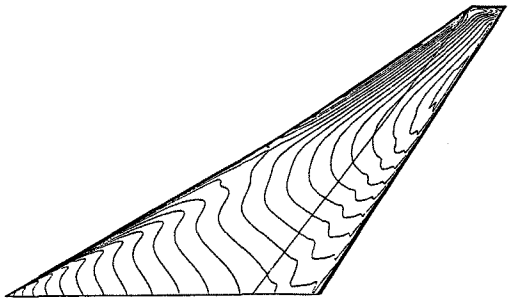

(d)
blunt leading edge wing
$M_\infty = 2.16, \alpha = 5°$

Fig. 10
Isobars on the upper wing surface ($\Delta c_p = 0.008$)

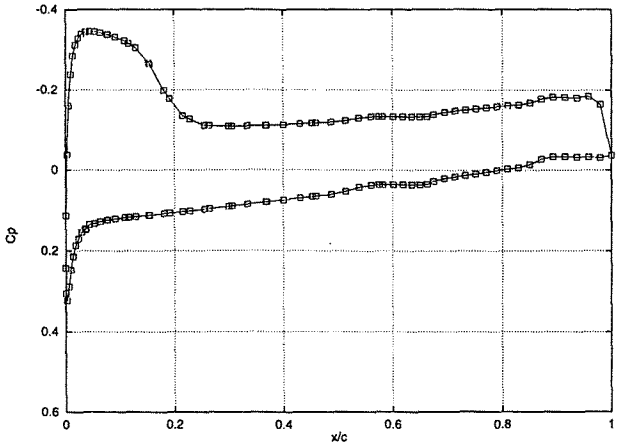

y/(b/2) = 0.3

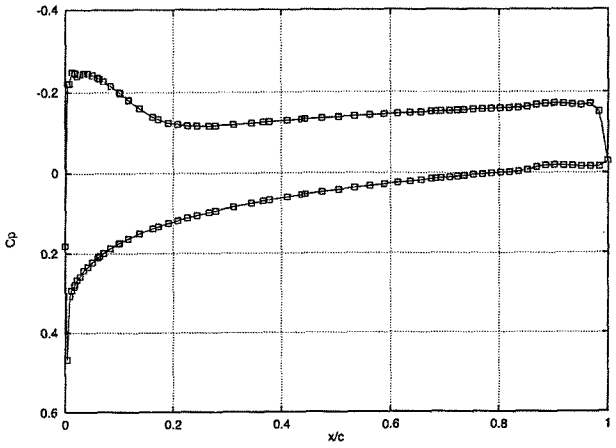

y/(b/2) = 0.3

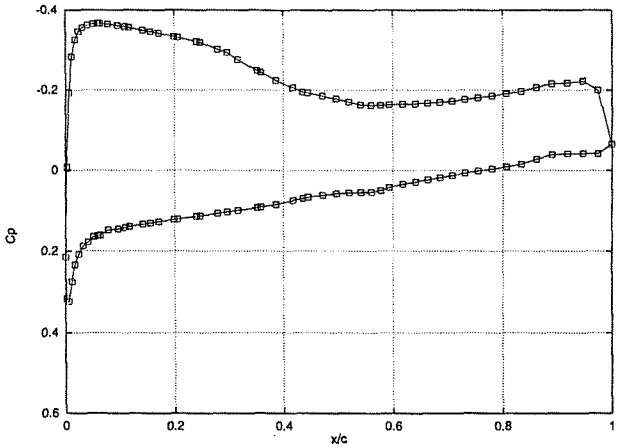

y/(b/2) = 0.5

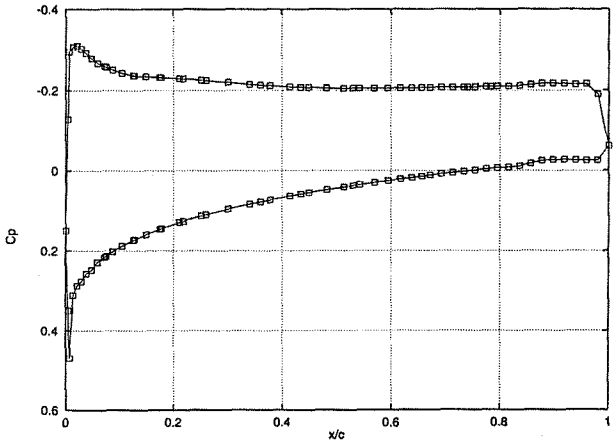

y/(b/2) = 0.5

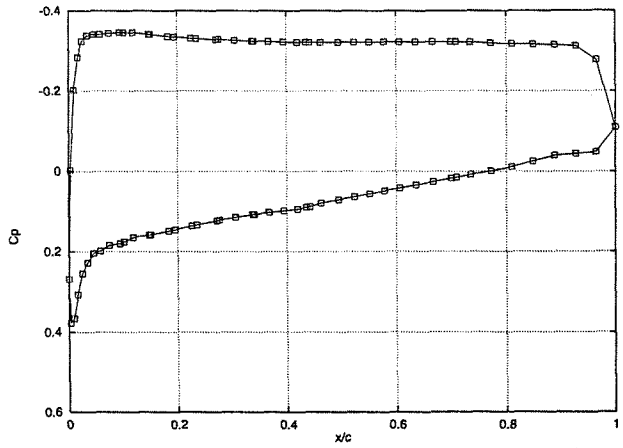

y/(b/2) = 0.7

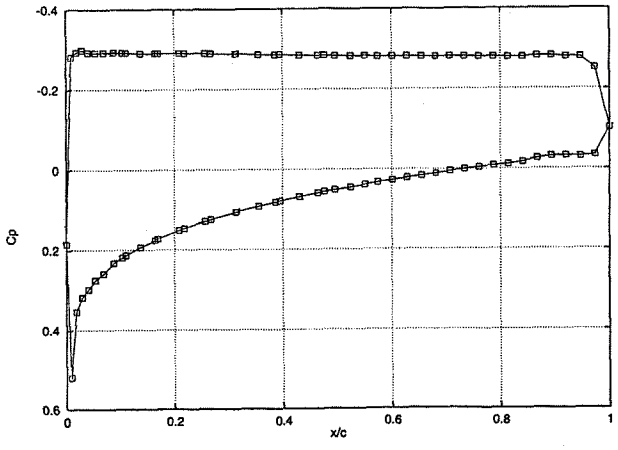

y/(b/2) = 0.7

Fig. 11
Pressure distribution at different spanwise sections
$M_\infty = 1.6, \alpha = 5°$
(a) blunt leading edge, (b) sharp leading edge

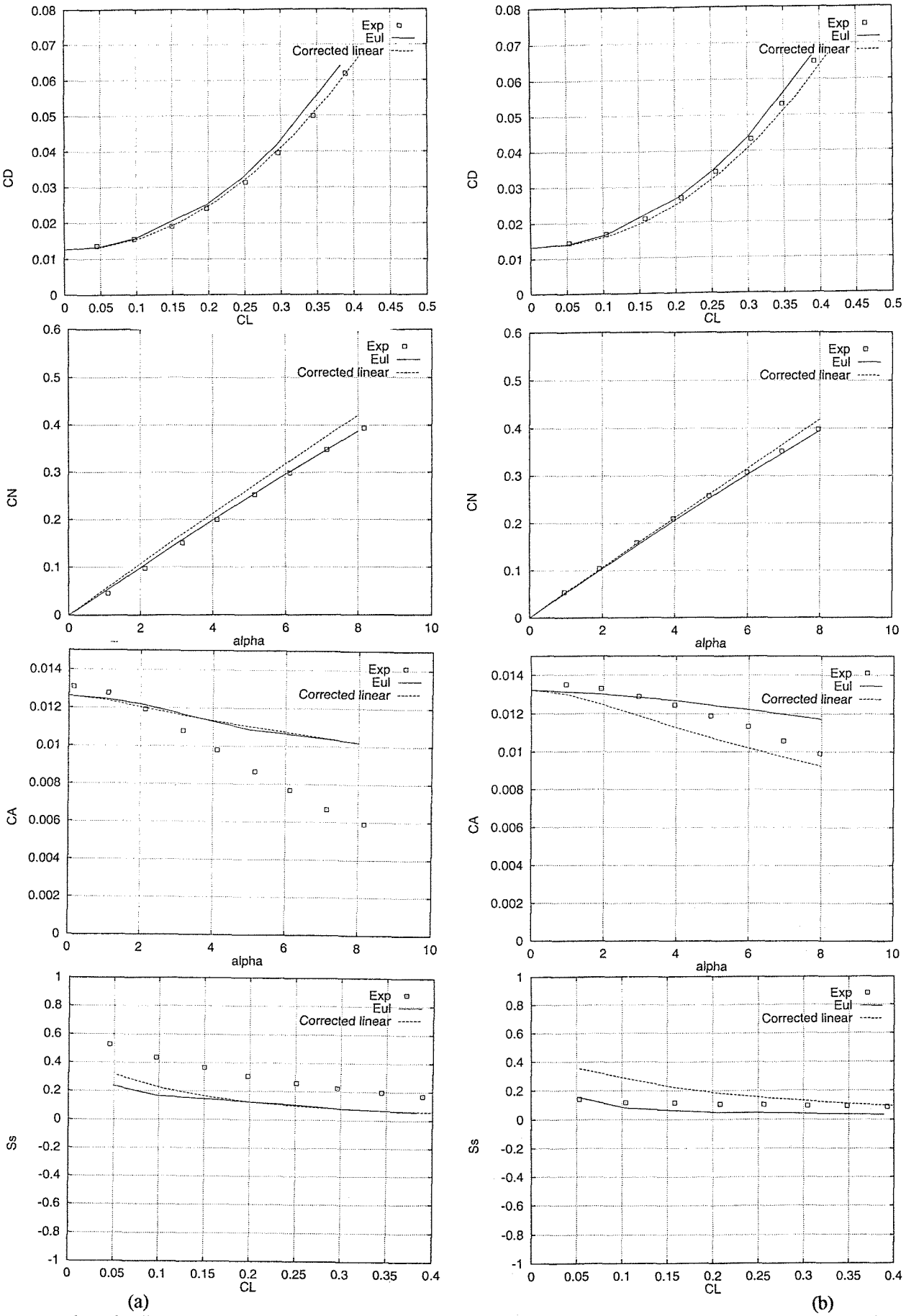

(a) sharp leading edge

(b) blunt leading edge

Fig. 12
Force coefficients ($M_\infty = 1.6$)

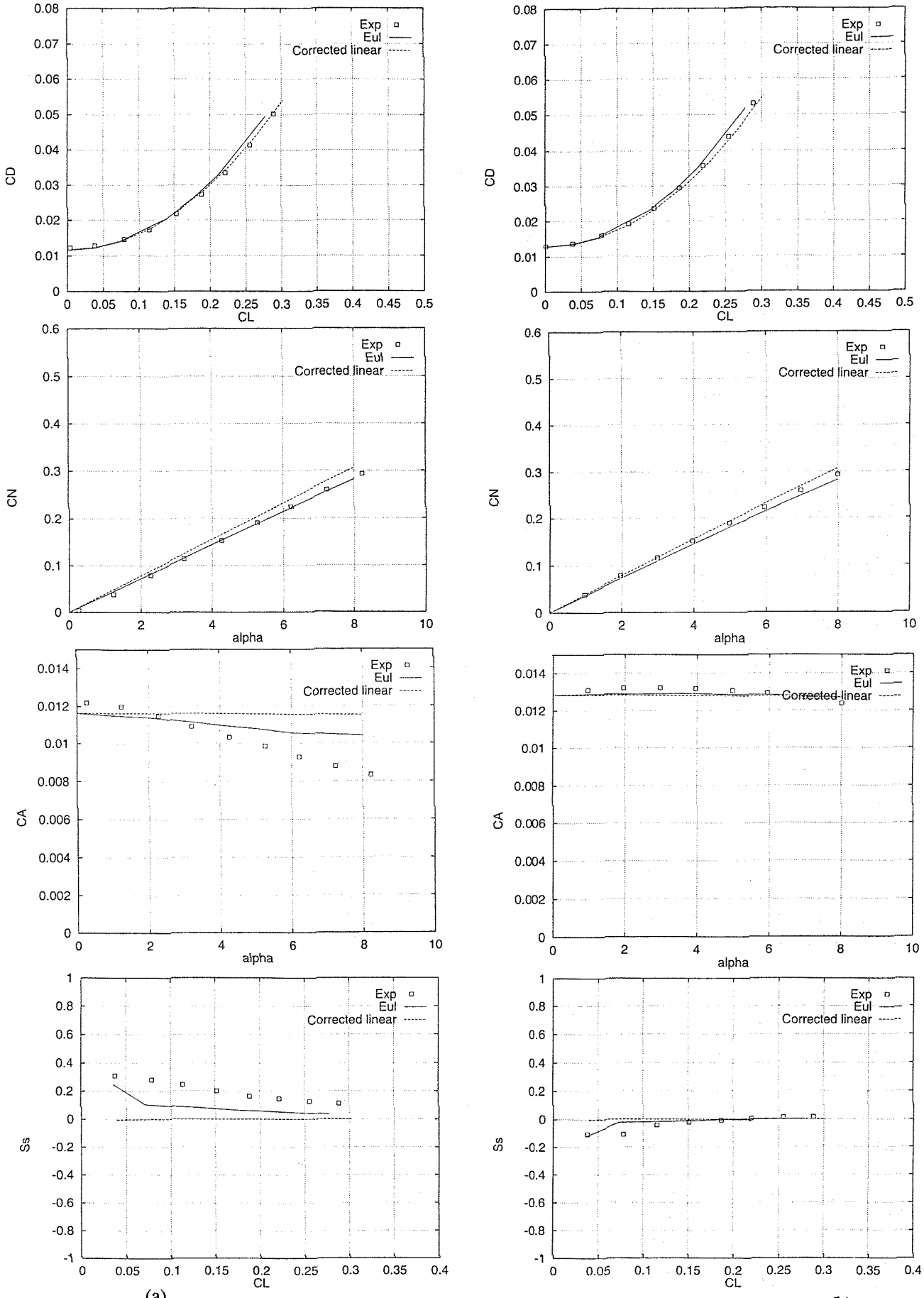

(a) sharp leading edge

(b) blunt leading edge

Fig. 13
Force coefficients ($M_\infty = 2.16$)